



1 Progressive groundwater decoupling may drive a shift toward 2 shallower and faster terrestrial water cycling

3 Aoqi Sun^{1†}, Wenjie Xu^{1†}, Enze Ma², Hua Yuan¹, Chen Yang^{1*}

4 1 School of Atmospheric Sciences, Sun Yat-sen University, Zhuhai, China

5 2 College of Soil and Water Conservation Science and Engineering, Northwest A&F University,

6 Yangling, China

7 †These authors contributed equally to this work

8 *Corresponding to: yangch329@mail.sysu.edu.cn

9 Abstract

10 Groundwater is widely regarded as a critical buffer that sustains evapotranspiration (ET) and
11 streamflow under hydrologic stress. However, whether this buffering capacity persists under
12 sustained increases in ET demand remains unclear. Here we test whether sustained increases in ET
13 demand can reorganize subsurface connectivity and undermine effective groundwater buffering,
14 using controlled hillslope simulations with integrated hydrologic modeling and particle tracking.
15 Under baseline semi-arid forcing, ET and outflow exhibit coexisting young and older age
16 components. Following late-summer groundwater drawdown, intermediate-age flow paths weaken,
17 eventually producing a temporary age gap that separates shallow and deep sources. Streamflow
18 responds more abruptly than ET due to hydraulic disconnection at the outlet. Warming and
19 vegetation greening amplify this intrinsic seasonal tendency. Intermediate-age contributions
20 collapse earlier and recover more slowly, amplifying the polarization between shallow and deep
21 water pools and further suppressing older groundwater inputs. Streamflow becomes increasingly
22 dominated by very young water, indicating strengthened groundwater–surface decoupling. These
23 results suggest that sustained hydrologic stress structurally reduces effective groundwater
24 connectivity, weakening subsurface buffering and shortening hydrologic memory. This tendency
25 persists across parameter perturbations. As a consequence, water cycling shifts toward shallower
26 and faster pathways. Progressive groundwater decoupling therefore represents not merely a change
27 in source depth, but a structural transition toward a more rapidly recycled and potentially less
28 predictable mode of terrestrial water cycling under sustained increases in terrestrial water use.



29 1. Introduction

30 Many terrestrial systems are increasingly exposed to hydrologic stress as atmospheric evaporative
31 demand intensifies and biological water use expands. In this context, warming and vegetation
32 enhancement act to amplify evapotranspiration (ET), increasing subsurface water extraction and
33 tightening constraints on groundwater storage.

34 Groundwater is widely regarded as a critical buffer against such hydrologic stress (Condon et al.,
35 2020; Miguez-Macho & Fan, 2025). By acting as a long-term storage reservoir and maintaining
36 hydraulic connectivity with the shallow subsurface, groundwater regulates the timing and
37 magnitude of surface water fluxes (Tran et al., 2020; Villaruel et al., 2025; Xie et al., 2024; Zipper
38 et al., 2024), sustains ET and streamflow during dry periods, and provides hydrologic “memory”
39 to the land surface system (Bierkens & van den Hurk, 2007; Brooks et al., 2021; Getirana et al.,
40 2025; Liang et al., 2021). Under this prevailing view, drought is interpreted as a progressive shift
41 toward deeper groundwater reliance: as shallow soil moisture is depleted, groundwater
42 contributions increase, leading to older water signatures in both ET and streamflow due to the
43 growing dominance of longer-residence subsurface water (Li et al., 2024; Swenson et al., 2024;
44 Visser et al., 2019; C. Yang et al., 2023; X. Yang et al., 2021). Implicit in this interpretation is the
45 tendency to assume that groundwater buffering remains effective even under sustained and
46 intensifying hydrologic stress.

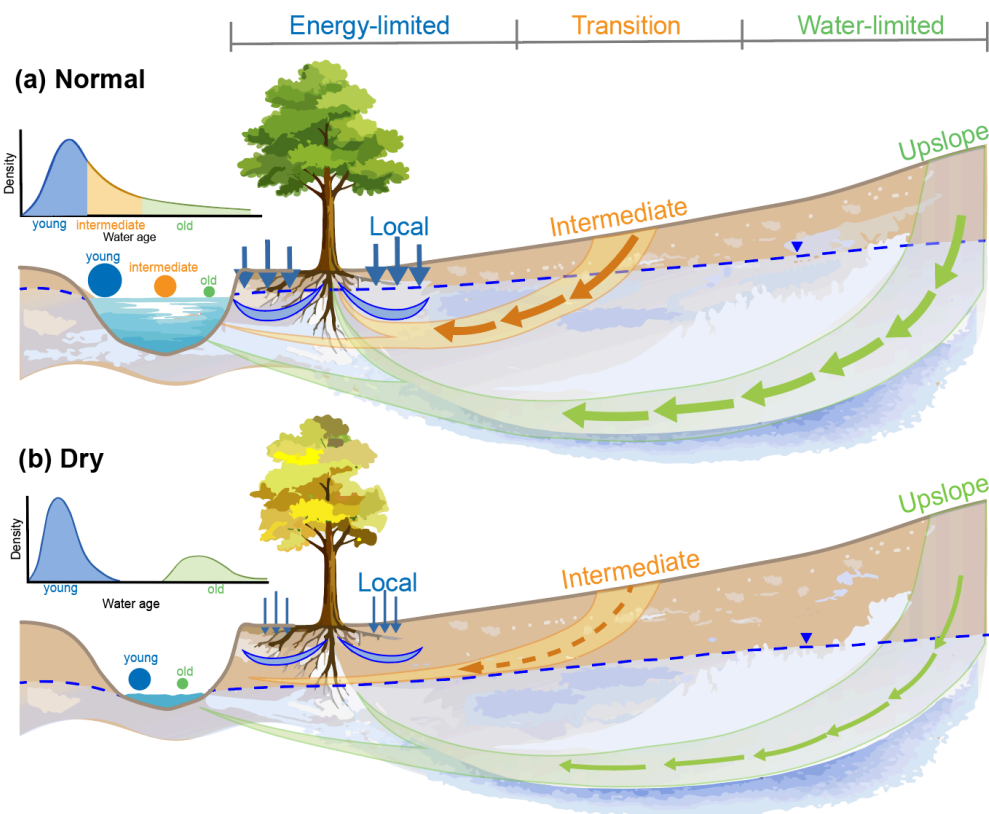
47 Using a high-resolution, observation-constrained integrated hydrologic model of the East River
48 headwaters in the Upper Colorado River basin, Carroll et al. (2024) examined how sustained
49 warming alters groundwater–stream interactions in a snow-dominated mountain system. Their
50 simulations indicate that progressive groundwater storage decline lowers regional water tables and
51 weakens hydraulic gradients toward stream channels, with some reaches shifting from historically
52 groundwater-gaining to losing or weakly connected states during low-flow periods. These results
53 suggest that sustained climatic stress may reorganize groundwater–surface water exchange
54 regimes. Similarly, Knighton and Berghuijs (2023), in a large-sample analysis of 472 U.S.
55 watersheds, linked ET water age to long-term ET magnitude and ecosystem drought resilience.
56 Watersheds characterized by older ET water tended to exhibit higher long-term ET but slower
57 post-drought recovery, whereas systems dominated by younger ET water showed greater resilience.
58 While focused on watershed-scale ET age rather than groundwater connectivity, these findings
59 indicate that water age metrics capture structural aspects of ecosystem water use under stress.

60 Taken together, these studies indicate that sustained hydrologic stress may alter not only the
61 magnitude of water fluxes, but also the depth and pace at which water circulates through terrestrial
62 systems. The East River simulations demonstrate that groundwater storage decline can weaken
63 deep groundwater contributions to streams, while the large-sample analysis of ET water age
64 suggests that reliance on older water is not necessarily enhanced under stress and may instead be
65 associated with reduced resilience. Rather than supporting the prevailing expectation that
66 intensifying drought strengthens groundwater buffering and progressively shifts fluxes toward
67 older water, these findings imply a different tendency: prolonged stress may reduce the effective
68 contribution of deeper storage and favor younger, more rapidly recycled water sources. **This**
69 **possibility raises a broader and largely unresolved question: can sustained hydrologic stress**



70 **shift terrestrial water cycling toward a shallower and faster regime, rather than simply**
 71 **intensifying groundwater dependence?**

72 Here we hypothesize that persistent increases in ET demand may shift terrestrial water cycling
 73 toward shallower and faster pathways, manifested through a systematic reorganization of internal
 74 water age structure. As groundwater storage declines beyond a critical threshold, intermediate-age
 75 contributions may collapse, leading to a separation between shallow, rapidly recycled water and
 76 deeper, longer-residence storage (**Figure 1**). This age polarization reflects a weakening of
 77 hydraulic connectivity between deep and shallow domains and signals a shift from a coupled
 78 regime—where multiple storage pools jointly regulate surface fluxes—to a decoupled regime
 79 dominated by shallower and faster flow paths.



80

81 **Figure 1. Shift from coupled to segregated flow structure with age polarization under**
 82 **groundwater decline. Arrows illustrate dominant source regions rather than exact flow**
 83 **trajectories**

84 To examine this possibility, we design a set of controlled hillslope experiments that systematically
 85 increase ET forcing and track the resulting evolution of water storage partitioning and water age
 86 structure. The hillslope represents the fundamental hydrologic unit (Fan et al., 2019) where vertical



87 and lateral processes interact, and subsurface flow organization is most directly expressed. By
88 isolating this elementary unit under realistic meteorological forcing, we focus on diagnosing the
89 intrinsic reorganization of age-structured water cycling under increasing ET demand. This
90 controlled configuration enables clear diagnosis of mechanism, providing a baseline understanding
91 that can inform interpretation of more complex real-world systems where multiple interacting
92 processes operate simultaneously.

93 2. Methods

94 To examine how enhanced ET forcing influences subsurface storage partitioning and internal
95 water age distribution, we conducted controlled numerical experiments in a synthetic quasi-three-
96 dimensional domain (Bearup et al., 2016; Danesh-Yazdi et al., 2018; Mikkelsen et al., 2013). The
97 domain represents a 100 m long, 1 m wide, and 9.4 m deep hillslope with a uniform surface
98 gradient of 0.1 (Figure S3). Although resolved in three dimensions, the narrow across-slope width
99 emphasizes dominant along-slope subsurface flow and lateral groundwater dynamics.

100 The hillslope was discretized using a terrain-following grid (Maxwell, 2013) at 5 m resolution
101 along-slope and 0.2 m across-slope, with 20 vertical layers of variable thickness: 0.5 m in the
102 deeper subsurface, gradually refining to 0.3 m and 0.1 m near the surface to better resolve shallow
103 processes. The land surface was prescribed as tree-covered vegetation representative of semi-arid
104 woody hillslopes. The upper 10 layers (4.4 m) constitute the root zone, where ParFlow and CLM
105 exchange water fluxes. This configuration enables explicit representation of vegetation uptake and
106 shallow soil moisture dynamics, while maintaining fully coupled groundwater flow beneath.

107 Subsurface hydraulic properties were specified uniformly (Maxwell et al., 2019; Yang et al., 2022).
108 Saturated hydraulic conductivity was set to 0.05 m h^{-1} , porosity to 0.20, and van Genuchten
109 parameters to $\alpha = 1.0 \text{ m}^{-1}$ and $n = 2$, and residual saturation (S_{res}) to 0.2. These geometric and
110 hydraulic specifications define a physically consistent semi-arid hillslope suitable for examining
111 structural shifts in subsurface water cycling under controlled forcing.

112 Water fluxes were simulated using the integrated hydrologic model ParFlow–CLM (Kollet &
113 Maxwell, 2006, 2008; Maxwell & Miller, 2005), which resolves coupled land surface processes
114 and variably saturated subsurface flow with lateral groundwater dynamics. The system was forced
115 with a representative semi-arid meteorological record characteristic of Oklahoma (USA),
116 providing realistic atmospheric demand and precipitation variability for a water-limited hillslope
117 environment (Kollet & Maxwell, 2008; Maxwell et al., 2019). The model was spun up for three
118 years, and the third-year state was used to initiate particle tracking. EcoSLIM (Maxwell et al.,
119 2019; Yang et al., 2022; C. Yang et al., 2021) simulations were then conducted for 20 years to
120 allow age distributions to approach dynamic equilibrium. All ParFlow–CLM and EcoSLIM
121 simulations were performed with an hourly time step.

122 EcoSLIM uses the transient flow fields and ET fluxes generated by ParFlow–CLM to simulate
123 particle advection and molecular diffusion, thereby explicitly tracking the transport pathways and
124 residence times of water within the coupled land–groundwater system. Diagnostics were derived
125 from the twentieth year. During the final analysis year, the domain consistently contained on the
126 order of 10^6 actively circulating particles. Over the course of that year, 2.17×10^5 particles exited



127 the domain as subsurface outflow and 2.48×10^5 were removed via ET. Because particle inflow
128 and release were continuous, the in-domain particle population remained approximately constant
129 while flux-specific particles were sampled as they exited. This high particle density and sustained
130 turnover enable robust, high-resolution characterization of flux age structure under different ET
131 forcing scenarios.

132 Building upon this baseline configuration, four primary forcing scenarios were constructed: a
133 baseline case, a $+1$ °C warming perturbation, a 50% increase in maximum leaf area index (LAI),
134 and a combined warming–greening scenario. The LAI perturbation magnitude reflects an
135 enhanced yet realistic continuation of observed multi-decadal greening trends (Piao et al., 2020),
136 while the $+1$ °C warming represents a moderate future climate signal (Ipcc, 2021).

137 To evaluate structural robustness, three additional experimental groups were conducted in which
138 key system properties were modified relative to the reference parameter set. In the first group,
139 vegetation type was changed from trees to shrubs, representing shallower rooting systems and
140 reduced transpiration demand. In the second group, subsurface hydraulic parameters were adjusted,
141 with saturated hydraulic conductivity set to 0.1 m h^{-1} , porosity to 0.39, van Genuchten parameters
142 to $\alpha = 3.5 \text{ m}^{-1}$ and $n = 2$, and S_{res} to 0.01 (Mikkelsen et al., 2013), representing a transition from
143 relatively low-porosity, semi-arid soils to more permeable, coarse-textured subsurface conditions.
144 In the third group, hillslope gradient was reduced to 0.05, representing weaker topographic control
145 on lateral drainage and groundwater convergence. In total, four experimental groups comprising
146 sixteen scenario combinations were simulated, each employing particle tracking to characterize
147 the evolution of subsurface water age structure.

148 **3. Results**

149 **3.1. Water fluxes**

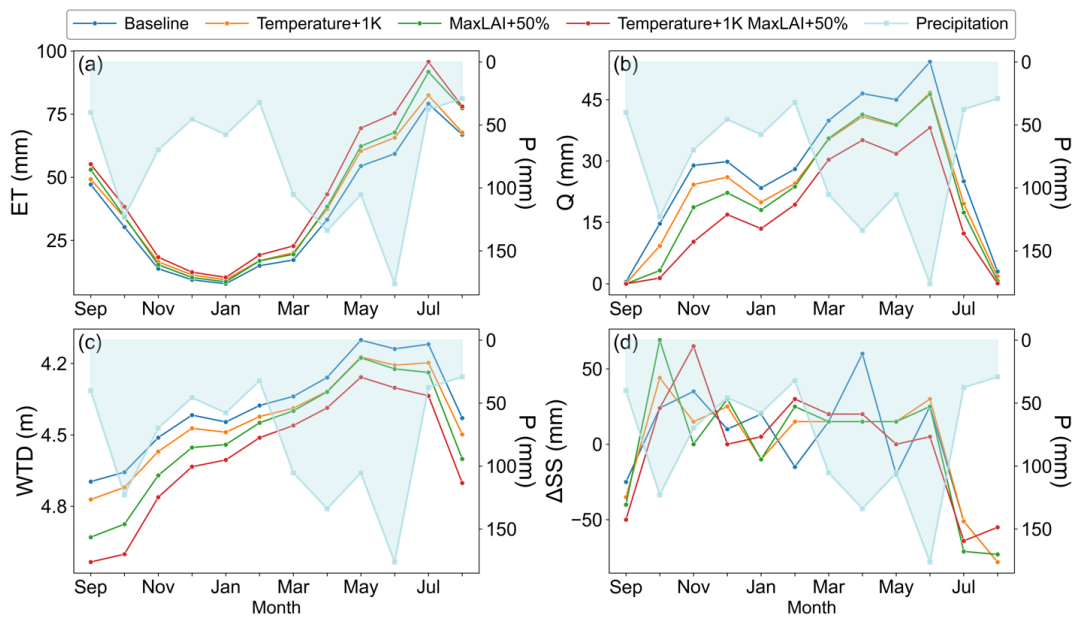
150 Under baseline conditions, seasonal water fluxes exhibit a pronounced late-summer transition
151 governed by the interaction between groundwater storage and ET demand (**Figure 2**). Following
152 gradual recovery during winter and spring, groundwater levels continue to rise and reach their
153 shallowest condition between May and July (**Figure 2c**). Air temperature increases after early
154 spring (**Figure S1**), and following a rainfall event in June, ET reaches its annual maximum in July
155 (**Figure 2a**).

156 The July ET peak triggers a rapid groundwater decline. With relatively modest rainfall in July and
157 August, groundwater drawdown continues even though ET weakens slightly in August; ET
158 remains substantial through August–September, pushing the water table to its annual maximum
159 depth in September (deepest condition). Consistent with this progression, saturated storage shows
160 pronounced net losses over July–September (**Figure 2d**), indicating that ET during this period is
161 supported in part by groundwater withdrawal. Concurrently, the domain-averaged ET age
162 increases (**Figure 3a**), consistent with greater reliance on older subsurface storage.

163 After September, ET declines from late-summer levels (September) and continues decreasing
164 through autumn (October–November), reaching a minimum in mid-winter (December–January),
165 before gradually increasing again in late spring (April–May). Although precipitation remains

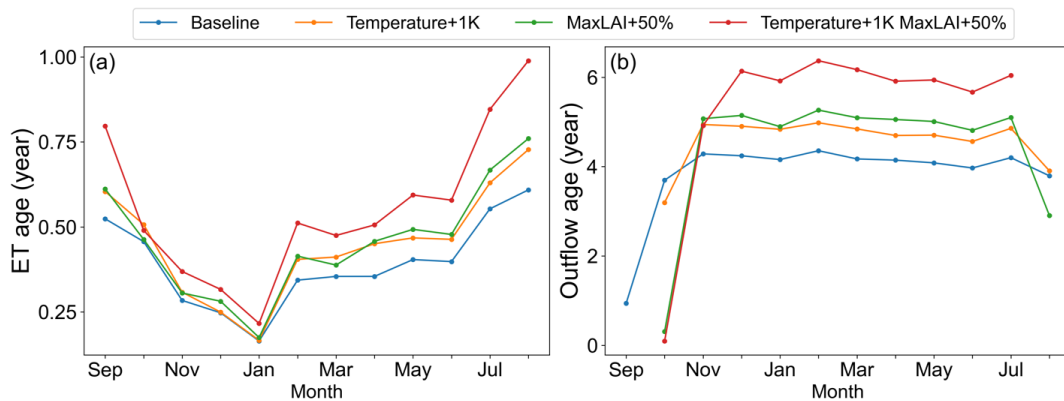


166 moderate during autumn and winter (October–February), both atmospheric demand and vegetation
 167 activity are strongly reduced (**Figure S1**). Lower air temperature suppresses evaporative demand,
 168 while reduced LAI during the dormant season limits transpiration, jointly constraining ET. As a
 169 result, water inputs exceed atmospheric losses during this period, allowing groundwater storage to
 170 progressively recover from autumn through spring, with groundwater levels becoming shallow
 171 again by May.



172

173 **Figure 2. Monthly precipitation (P), evapotranspiration (ET), streamflow (Q), water table**
 174 **depth (WTD), and saturated storage change (Δ SS) under baseline and enhanced ET forcing**



175

176 **Figure 3. Monthly mean ET and outflow ages under different ET forcing scenarios**



177 Streamflow closely tracks seasonal groundwater dynamics (**Figure 2b**). Discharge reaches its
178 annual maximum in June, when groundwater levels are shallow, and declines toward a minimum
179 in September as the water table reaches its deepest condition. In contrast to the maximum ET age
180 observed during late-summer groundwater drawdown, outflow age exhibits the opposite tendency
181 during August–October, declining sharply as streamflow becomes dominated by very young water
182 (**Figure 3b**). This age decrease reflects hydraulic disconnection between the channel and deeper
183 groundwater once the water table drops below the outlet elevation (**Figure S2**), effectively
184 suppressing older groundwater contributions.

185 In addition to the late-summer minimum in outflow, two secondary discharge declines are evident
186 (**Figure 2b**): one in January and another in May. The January dip reflects a delayed drainage
187 adjustment following enhanced recharge and temporarily strengthened hydraulic connectivity in
188 autumn. After the October rainfall temporarily increases subsurface water availability, the system
189 undergoes accelerated drainage through November and December, progressively depleting stored
190 water. By January, despite a modest precipitation peak, discharge declines because much of the
191 transiently accumulated storage has already been drained (**Figure S3**). The May reduction, in
192 contrast, corresponds to a sharp increase in ET relative to April. As atmospheric demand rises and
193 vegetation activity resumes, increased ET suppresses groundwater discharge, producing a
194 secondary decline before peak flow is reached in June.

195 This seasonal transition sets the stage for the structural reorganization of internal water age
196 described below.

197 **3.2. Age distributions**

198 Under baseline conditions, ET and outflow exhibit two persistent age components: young, locally
199 recharged water and older groundwater-sourced water (**Figures 4–6 and S4–S6**). These
200 components vary seasonally but generally coexist. Although ET ages are computed across the
201 entire hillslope, the discussion below focuses on the downslope portion (approximately the lower
202 20 m). In this zone, soil saturation remains close to unity for much of the year (**Figure S3**),
203 maintaining strong lateral convergence and vertical hydraulic connectivity across the profile. The
204 shallow subsurface therefore remains well coupled to deeper groundwater storage, and water
205 availability is rarely limiting. As a result, the ET age spectrum in this region reflects contributions
206 from both locally recharged downslope water and older upslope groundwater storage.

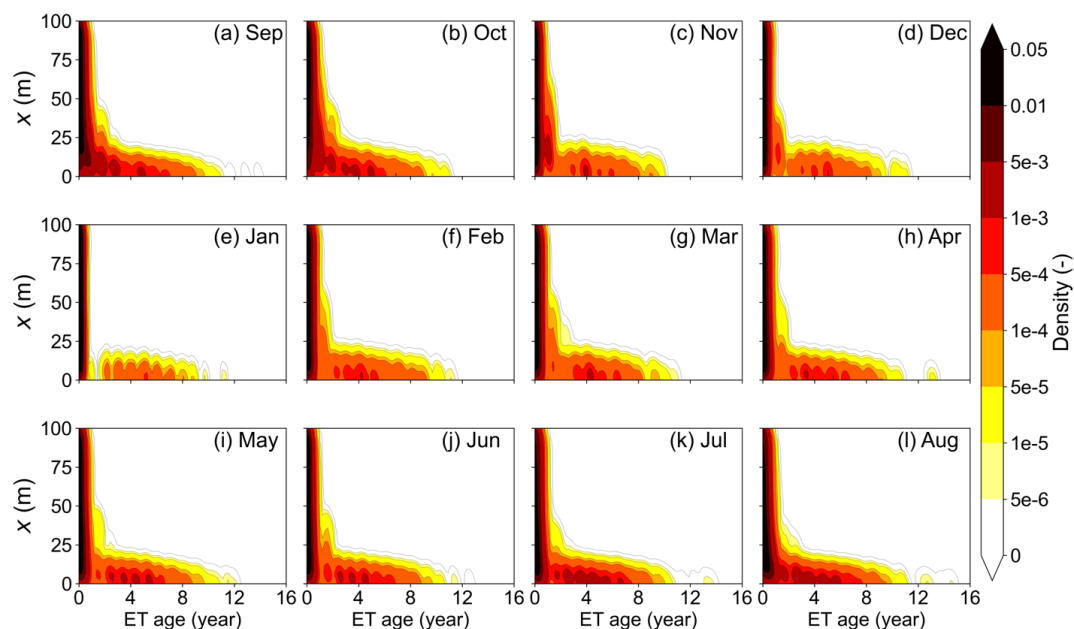
207 Particle source diagnostics further confirm this spatial separation of age components. ET particles
208 with ages between 0.5–1 year predominantly originate within the lower ~20 m of the hillslope,
209 indicating a locally recharged downslope water source (**Figure S7**). In contrast, particles with ages
210 between 1–2.5 years are traced to positions upslope of 20 m, demonstrating that older ET
211 contributions are supplied by more distal upslope groundwater storage (**Figure S8**). This age-
212 dependent upslope shift in source location confirms that the two age components correspond to
213 locally recharged downslope water and older upslope groundwater storage.

214 Following the late-summer drying (around September), the water table deepens. As the system
215 desaturates, intermediate subsurface flow paths that connect shallow storage to deeper
216 groundwater weaken. In the subsequent months, ET remains at a moderate level and continues to



217 draw partly on deeper soil water, so the intermediate-age component does not vanish immediately.
 218 However, as ET gradually decreases toward winter, its reliance on deeper water diminishes and
 219 the contribution of locally stored shallow water becomes more prominent. This seasonal shift in
 220 water use progressively reduces the relative contribution of older water in the ET age distribution,
 221 as reflected by the gradual fading of high-density colors in the older age range (**Figures 4 and 5**).

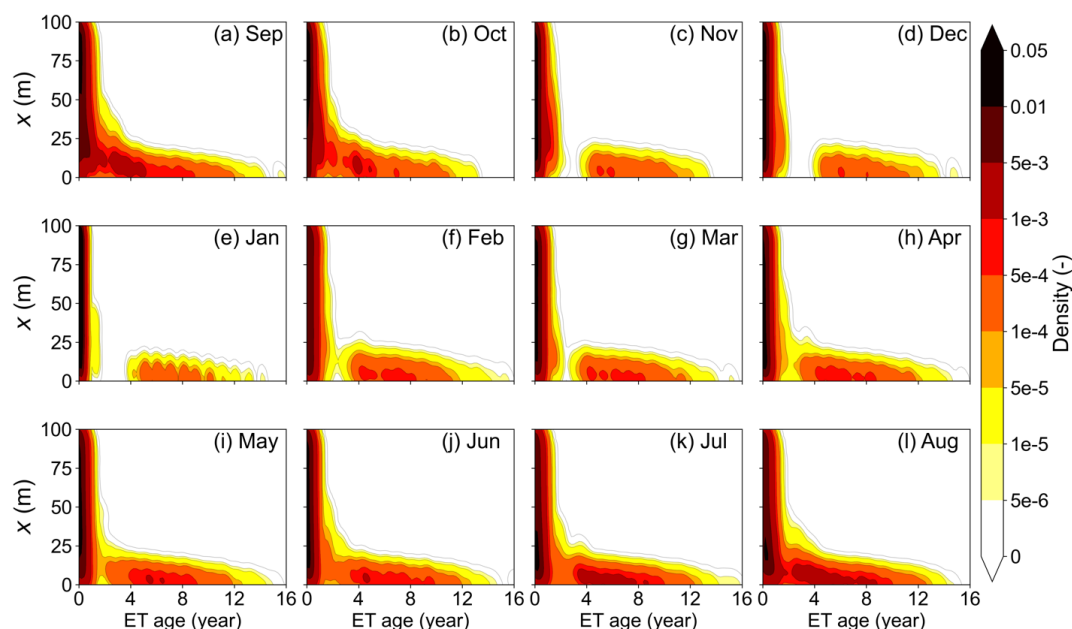
222 By January, when ET demand is minimal, water use is largely confined to shallow near-surface
 223 storage (**Figure S9**). Meanwhile, portions of the intermediate-age water stored in deeper soil layers
 224 were reduced during transient drainage in the preceding months, and the delayed drying signal
 225 from upslope areas has propagated downslope. The combined effect of prior drainage and delayed
 226 signal transmission results in a temporary loss of intermediate-age contributions, producing the
 227 pronounced age gap observed in early winter (January, **Figures 4 and 5**). Notably, this age-gap
 228 formation coincides with the January dip in streamflow (**Figure 2b**), indicating that the short-lived
 229 autumn recharge did not fully reverse the preceding drying signal.



230

231 **Figure 4. Monthly spatial distribution of ET age along the hillslope under baseline conditions**

232



233

234 **Figure 5. Monthly spatial distribution of ET age along the hillslope under combined**
 235 **warming-greening forcing**

236 Particle source diagnostics (**Figure 7**) reveal two spatially distinct ET source regions, with
 237 contributions originating from both proximal downslope storage and more distal upslope portions
 238 of the hillslope. Following late-summer depletion, contributions from the slope segment
 239 immediately upslope of the lower 20 m zone are markedly reduced. This segment corresponds to
 240 the transition from energy-limited to water-limited conditions (**Figure S10**) and represents a key
 241 bridging pathway linking deeper upslope storage to downslope ET (**Figure 1**). ET increases
 242 markedly along the downslope transition zone (approximately 20–60 m), particularly during July–
 243 September (**Figure S10**). However, soil saturation in this region does not reach the more favorable
 244 moisture conditions observed at the hillslope toe (lower 20 m, **Figure S3**), rendering it more
 245 vulnerable to moisture limitation during dry or drought periods. This vulnerability likely disrupts
 246 intermediate subsurface flow paths, contributing to the observed contraction of bridging
 247 connectivity and the emergence of the ET age gap.

248 Streamflow responds more abruptly than ET. In September, groundwater levels reach their annual
 249 minimum, and at the hillslope outlet the water table drops below the land surface elevation,
 250 effectively disconnecting deeper groundwater from the channel. As a result, older groundwater
 251 contributions rapidly diminish, leaving streamflow dominated by very young, locally recharged
 252 water generated primarily through saturation-excess runoff (**Figure 6a**).

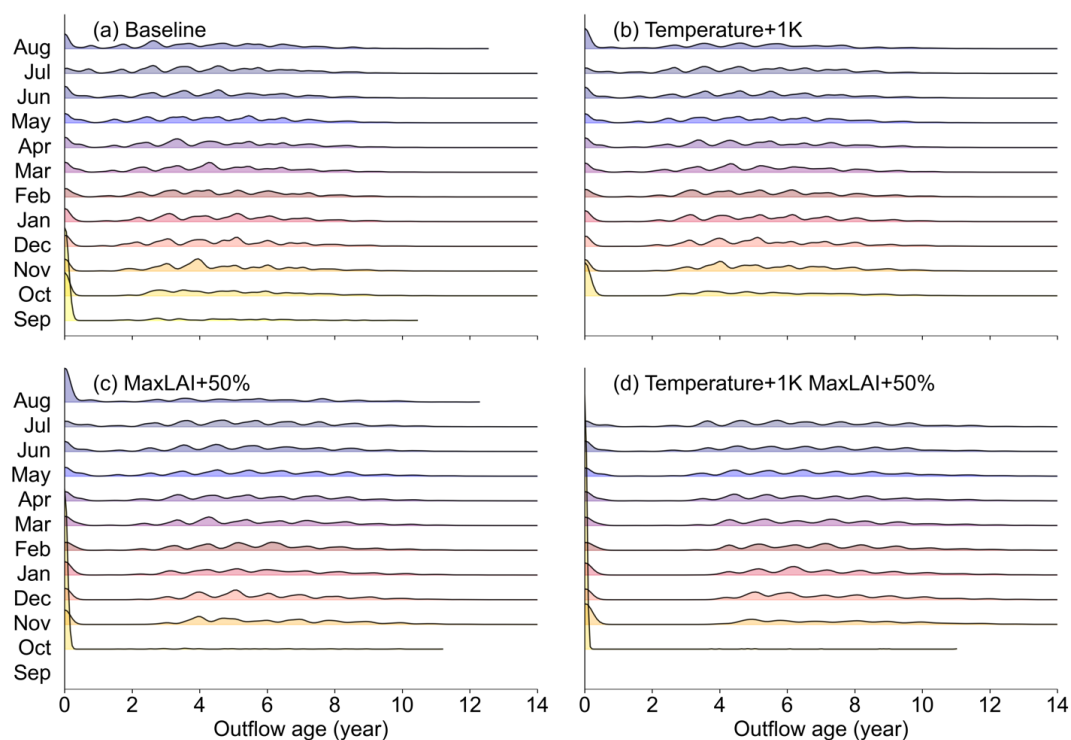
253 As precipitation increases in October, older groundwater contributions begin to reappear at the
 254 outlet. However, this re-emergence remains separated from the young component by a pronounced
 255 age gap, reflecting the incomplete recovery of intermediate-age contributions (**Figure 6a**). Unlike



256 ET, which can actively tap locally stored deeper soil water through root uptake and thus
257 temporarily retain intermediate-age contributions, streamflow behaves as a passive drainage flux.
258 Once hydraulic connectivity weakens, intermediate-age contributions decline immediately and
259 remain suppressed until subsurface connectivity is progressively restored through seasonal
260 recharge.

261 By mid-winter (January–February), the earlier drying signal has largely drained through the system,
262 while concurrent recharge gradually rebuilds storage (**Figure 6a**). Consequently, the age gap
263 narrows progressively through late winter and spring, signaling the seasonal reactivation of
264 intermediate pathways and the gradual restoration of subsurface connectivity.

265

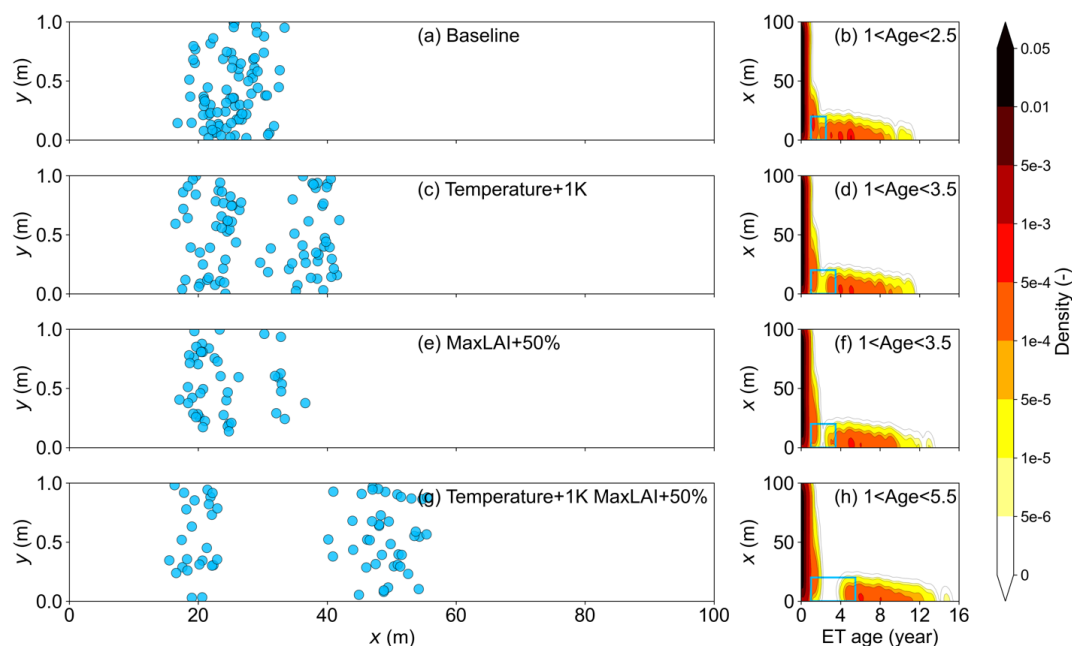


266

267 **Figure 6. Monthly outflow age distributions under four ET forcing scenarios**

268

269



270

271 **Figure 7. Source regions of ET particles (lower 20 m zone) for selected age ranges under**
 272 **different ET forcing scenarios**

273 3.3. Warming and greening

274 Warming and vegetation greening both intensify this seasonal reorganization of ET age structure.
 275 Under these scenarios, intermediate-age contributions collapse more abruptly during late summer,
 276 so that a clear age gap emerges earlier than in the baseline case and remains prominent through
 277 the subsequent months (**Figures S4–S5**). The combined warming–greening scenario shows the
 278 strongest amplification: a distinct separation between shallow and deep age components is already
 279 evident by November, and the two components remain largely disconnected through winter and
 280 spring. Only by the following May does a weak partial reconnection begin to appear, indicating a
 281 delayed and incomplete return of intermediate-age contributions (**Figure 5**). Overall, enhanced ET
 282 forcing advances the onset of age segregation and prolongs the period over which ET draws from
 283 two separated shallow and deep source pools.

284 Streamflow exhibits an even more abrupt response under warming and greening (**Figures 6b–6d**).
 285 In September, discharge effectively collapses. Under the combined warming–greening scenario,
 286 October outflow is almost entirely composed of very young water, with older groundwater
 287 contributions nearly absent and a pronounced age gap separating the young and older components.
 288 Throughout the following months, the reconnection between young and older components remains
 289 weak. Even into early summer (around May), the restoration of intermediate-age connectivity
 290 remains incomplete, indicating a delayed and structurally weakened recovery of groundwater–
 291 surface water coupling.



292 Importantly, these perturbations do not introduce a fundamentally new behavior, but amplify the
293 intrinsic seasonal tendency toward groundwater–surface decoupling already present under
294 baseline conditions. Warming and greening advance its onset, extend its duration, and in some
295 cases push the system toward a quasi-persistent decoupled regime. In addition to advancing the
296 onset of age segregation, warming and greening also enhance the polarization of the age spectrum,
297 with young components becoming increasingly concentrated at very short residence times while
298 older contributions are either shifted toward longer ages or temporarily suppressed. Taken together,
299 these patterns indicate that progressive groundwater decoupling under enhanced ET forcing drives
300 a shift toward faster and shallower terrestrial water cycling.

301 **3.4 Structural robustness across parameter configurations**

302 To evaluate whether the age-gap formation and deep–shallow decoupling depend on a specific
303 parameter choice, we examined three additional parameter groups involving vegetation type,
304 subsurface hydraulic properties, and hillslope gradient. Across all configurations, the qualitative
305 reorganization pathway identified under the reference parameter configuration remains evident,
306 although its magnitude varies. When vegetation was changed from trees to shrubs (**Figures S11–**
307 **S12**), overall ET demand and seasonal water stress were reduced. As expected, both ET and
308 outflow age structures became less polarized, and the seasonal age gap weakened, yet the
309 separation between shallow and deep contributions remained discernible. This behavior is
310 consistent with the stress-controlled nature of the mechanism: reduced water demand dampens,
311 but does not eliminate, connectivity-driven reorganization.

312 Modifying subsurface hydraulic properties (**Figures S13–S14**) altered the balance of connectivity
313 pathways without disrupting the underlying pattern. Higher saturated hydraulic conductivity and
314 porosity enhanced lateral groundwater movement toward the hillslope toe, increasing the relative
315 contribution of older groundwater to outflow. At the same time, larger α and lower residual
316 saturation weakened capillary linkage between the root zone and deeper storage, reducing the
317 older-water fraction in ET. As a result, outflow exhibited a greater proportion of old water, whereas
318 ET shifted toward younger sources. In both fluxes, the age gap remained detectable but
319 substantially muted, primarily reflecting a redistribution between young and old contributions. In
320 contrast, reducing hillslope gradient (**Figures S15–S16**) weakened both lateral drainage and
321 vertical hydraulic connectivity, amplifying seasonal decoupling. Under these conditions, old-water
322 contributions nearly vanished during winter months in both ET and outflow, and the age gap
323 became more pronounced during the rest of the year.

324 Together, these results indicate that parameter perturbations modulate the intensity and
325 manifestation of groundwater–surface decoupling, but do not alter the underlying reorganization
326 tendency. The emergence of age segregation under sustained stress therefore appears robust across
327 variations in vegetation, hydraulic properties, and slope gradient.

328 **4. Discussion**

329 Fan et al. (2017) has emphasized that vegetation water use is regulated by two hydrologic regimes:
330 shallow soil moisture supplied by rainfall infiltration and deeper groundwater accessible through
331 hydraulic connectivity. Similarly, tracer studies show that streamflow integrates a fast, young-



332 water regime and a slower, old-water regime linked to deeper storage (Florianoic et al., 2024). Our
333 findings refine this dual-regime perspective by showing that under dry or drought conditions,
334 declining hydraulic connectivity weakens the groundwater-controlled regime and may even lead
335 to partial decoupling from deeper storage. Importantly, this mechanism does not contradict
336 observations from many drought studies reporting an increase in the fraction of “old water” during
337 dry periods (von Freyberg et al., 2018; Wilusz et al., 2019). Even when groundwater contributions
338 diminish, the relative importance of deeper soil moisture within the infiltration-controlled regime
339 can increase, leading to slightly older effective source water. What we emphasize here is that the
340 deepest groundwater reservoir does not necessarily become progressively more engaged under
341 increasing stress; rather, its contribution may be suppressed as connectivity contracts (**Figure 1**).
342 While derived from controlled hillslope experiments, the mechanism identified here isolates a
343 fundamental reorganization pathway that may operate in real catchments under sustained stress.

344 The structural tendency identified here is unlikely to weaken under ongoing global change.
345 Sustained warming and widespread vegetation greening increase atmospheric and biological water
346 demand from above (Pokhrel et al., 2021; Y. Yang et al., 2023), while groundwater extraction
347 reduces subsurface storage from below (Jasechko et al., 2024). These combined pressures intensify
348 overall water stress and weaken deep–shallow hydraulic connectivity. The documented eastward
349 shift of the hydroclimatic dry–wet boundary along the 100th meridian west in North America—
350 reported to have migrated approximately 140 miles eastward since 1980 (Seager, Feldman, et al.,
351 2018; Seager, Lis, et al., 2018)—suggests that an expanding fraction of landscapes is becoming
352 increasingly water-limited, a condition under which subsurface connectivity is more prone to
353 weakening. Recurrent groundwater drought and widespread baseflow decline further reflect this
354 progressive loss of subsurface buffering (Elsaidy et al., 2025; Tan et al., 2020). Under such
355 conditions, contraction of intermediate flow paths and groundwater–surface decoupling may
356 become increasingly prevalent rather than exceptional.

357 A gradual loss of groundwater connectivity weakens the subsurface buffering capacity that
358 stabilizes surface fluxes. As deep storage becomes less engaged, the hydrologic memory carried
359 by long-residence water diminishes. Consequently, antecedent storage conditions exert a weaker
360 influence on subsequent ET and streamflow, and fluxes become more directly controlled by short-
361 term atmospheric forcing. With reduced temporal persistence, the capacity to infer future fluxes
362 from present storage states declines. At the same time, the diminished participation of deep storage
363 reduces the system’s ability to absorb and moderate climatic extremes, weakening its resilience.
364 Such a system is therefore both more sensitive to external forcing and inherently more difficult to
365 predict under sustained stress (Shi et al., 2022). Future work will examine how this structural
366 mechanism manifests in real catchments, where heterogeneity and multi-scale feedbacks interact
367 with groundwater connectivity under complex climatic and geomorphic conditions.

368 5. Summary

369 This study demonstrates that sustained increases in ET demand may fundamentally reorganize the
370 internal age structure of terrestrial water cycling. Using controlled hillslope experiments with
371 integrated hydrologic modeling and particle tracking, we show that progressive groundwater
372 storage decline weakens intermediate-age flow paths and separates shallow, rapidly recycled water
373 from deeper, long-residence storage. Under enhanced warming and greening, this seasonal age



374 polarization emerges earlier, persists longer, and becomes more pronounced, driving streamflow
375 and ET toward increasingly young water sources. This connectivity-driven tendency remains
376 evident across variations in vegetation type, soil hydraulic properties, and slope gradient. Rather
377 than progressively strengthening groundwater buffering under drought, sustained hydrologic stress
378 can suppress effective groundwater engagement, shorten hydrologic memory, and shift landscapes
379 toward a shallower and faster mode of water cycling. Progressive groundwater decoupling
380 therefore represents a structural transition in terrestrial water systems, with implications for
381 predictability, resilience, and water resource stability under ongoing climate and vegetation change.

382

383 **Code and data availability**

384 ParFlow version 3.14.1 was used in this study:

385 <https://github.com/parflow/parflow/archive/refs/tags/v3.14.1.zip>

386 EcoSLIM version 1.31 was employed for particle tracking:

387 <https://github.com/reedmaxwell/EcoSLIM/archive/refs/tags/v1.31.zip>

388 Minor modifications were made to the EcoSLIM source code to accommodate the experimental
389 configuration described here.

390 All ParFlow and EcoSLIM run scripts for the full set of scenarios, together with the post-
391 processing and figure-generation scripts, are available at

392 <https://doi.org/10.6084/m9.figshare.31410108>

393 **Author contribution**

394 Conceptualization: CY. Methodology: CY and AS. Investigation: CY, AS, and WX. Resources:
395 CY. Writing (original draft): CY, AS, and WX. Writing (review and editing): CY, AS, WX, EM,
396 and HY.

397 **Competing interests**

398 The contact author has declared that none of the authors has any competing interests.

399

400

401



477 References

- 478 Bearup, L. A., Maxwell, R. M., & McCray, J. E. (2016). Hillslope response to insect-induced
479 land-cover change: an integrated model of end-member mixing. *Ecohydrology*, 9(2), 195-
480 203. <Go to ISI>://WOS:000372309400001
481 Bierkens, M. F. P., & van den Hurk, B. J. J. M. (2007). Groundwater convergence as a possible
482 mechanism for multi-year persistence in rainfall. *Geophysical Research Letters*, 34(2).
483 <https://doi.org/10.1029/2006GL028396>
484 Brooks, P. D., Gelderloos, A., Wolf, M. A., Jamison, L. R., Strong, C., Solomon, D. K., Bowen,
485 G. J., Burian, S., Tai, X., Arens, S., Briefer, L., Kirkham, T., & Stewart, J. (2021).
486 Groundwater-Mediated Memory of Past Climate Controls Water Yield in Snowmelt-
487 Dominated Catchments. *Water Resources Research*, 57(10), e2021WR030605.
488 <https://doi.org/https://doi.org/10.1029/2021WR030605>
489 Carroll, R. W. H., Niswonger, R. G., Ulrich, C., Varadharajan, C., Siirila-Woodburn, E. R., &
490 Williams, K. H. (2024). Declining groundwater storage expected to amplify mountain
491 streamflow reductions in a warmer world. *Nature Water*, 2(5), 419-433.
492 <https://doi.org/10.1038/s44221-024-00239-0>
493 Condon, L. E., Atchley, A. L., & Maxwell, R. M. (2020). Evapotranspiration depletes
494 groundwater under warming over the contiguous United States. *Nature Communications*,
495 11(1), 873. <https://doi.org/10.1038/s41467-020-14688-0>
496 Danesh-Yazdi, M., Klaus, J., Condon, L. E., & Maxwell, R. M. (2018). Bridging the gap between
497 numerical solutions of travel time distributions and analytical storage selection functions.
498 *Hydrological Processes*, 32(8), 1063-1076. <Go to ISI>://WOS:000430466700006
499 Elsaidy, A., Yimer, E. A., Mogheir, Y., Huysmans, M., Villani, L., & van Griensven, A. (2025).
500 Groundwater drought and anthropogenic amplifiers: A review of assessment and response
501 strategies in arid and semi-arid areas. *Science of the Total Environment*, 978, 179406.
502 <https://doi.org/https://doi.org/10.1016/j.scitotenv.2025.179406>
503 Fan, Y., Clark, M., Lawrence, D. M., Swenson, S., Band, L. E., Brantley, S. L., Brooks, P. D.,
504 Dietrich, W. E., Flores, A., Grant, G., Kirchner, J. W., Mackay, D. S., McDonnell, J. J.,
505 Milly, P. C. D., Sullivan, P. L., Tague, C., Ajami, H., Chaney, N., Hartmann,
506 A.,... Yamazaki, D. (2019). Hillslope Hydrology in Global Change Research and Earth
507 System Modeling. *Water Resources Research*, 55(2), 1737-1772.
508 <https://doi.org/10.1029/2018wr023903>
509 Fan, Y., Miguez-Macho, G., Jobbágy, E. G., Jackson, R. B., & Otero-Casal, C. (2017).
510 Hydrologic regulation of plant rooting depth. *Proceedings of the National Academy of*
511 *Sciences*, 114(40), 10572-10577. <https://doi.org/10.1073/pnas.1712381114>
512 Floriatic, M. G., Allen, S. T., & Kirchner, J. W. (2024). Young and new water fractions in soil
513 and hillslope waters. *Hydrol. Earth Syst. Sci.*, 28(18), 4295-4308.
514 <https://doi.org/10.5194/hess-28-4295-2024>
515 Getirana, A., Kumar, S., & Rodell, M. (2025). Inconsistencies in GRACE-Based Groundwater
516 Storage Estimation—A Call for a Proper Use of Land Surface Models. *Geophysical*
517 *Research Letters*, 52(19), e2025GL119197.
518 <https://doi.org/https://doi.org/10.1029/2025GL119197>
519 Ippc. (2021). *Climate Change 2021: The Physical Science Basis. Contribution of Working Group*
520 *I to the Sixth Assessment Report of the Intergovernmental Panel on Climate Change* (Vol.
521 In Press). Cambridge University Press. <https://doi.org/10.1017/9781009157896>



- 522 Jasechko, S., Seybold, H., Perrone, D., Fan, Y., Shamsudduha, M., Taylor, R. G., Fallatah, O., &
523 Kirchner, J. W. (2024). Rapid groundwater decline and some cases of recovery in aquifers
524 globally. *Nature*, 625(7996), 715-721. <https://doi.org/10.1038/s41586-023-06879-8>
- 525 Knighton, J., & Berghuijs, W. R. (2023). Water Ages Explain Tradeoffs Between Long-Term
526 Evapotranspiration and Ecosystem Drought Resilience. *Geophysical Research Letters*,
527 50(10), e2023GL103649. <https://doi.org/https://doi.org/10.1029/2023GL103649>
- 528 Kollet, S. J., & Maxwell, R. M. (2006). Integrated surface-groundwater flow modeling: A free-
529 surface overland flow boundary condition in a parallel groundwater flow model.
530 *Advances in Water Resources*, 29(7), 945-958. <Go to ISI>://WOS:000238830800001
- 531 Kollet, S. J., & Maxwell, R. M. (2008). Capturing the influence of groundwater dynamics on
532 land surface processes using an integrated, distributed watershed model. *Water Resources*
533 *Research*, 44(2). https://doi.org/Artn_W0240210.1029/2007wr006004
- 534 Li, L., Knapp, J. L. A., Lintern, A., Ng, G. H. C., Perdrial, J., Sullivan, P. L., & Zhi, W. (2024).
535 River water quality shaped by land–river connectivity in a changing climate. *Nature*
536 *Climate Change*, 14(3), 225-237. <https://doi.org/10.1038/s41558-023-01923-x>
- 537 Liang, X., Schilling, K. E., Jones, C. S., & Zhang, Y.-K. (2021). Temporal scaling of long-term
538 co-occurring agricultural contaminants and the implications for conservation planning.
539 *Environmental Research Letters*, 16(9), 094015. <https://doi.org/10.1088/1748-9326/ac19dd>
- 540 Maxwell, R. M. (2013). A terrain-following grid transform and preconditioner for parallel, large-
541 scale, integrated hydrologic modeling. *Advances in Water Resources*, 53, 109-117.
542 <https://doi.org/https://doi.org/10.1016/j.advwatres.2012.10.001>
- 543 Maxwell, R. M., Condon, L. E., Danesh-Yazdi, M., & Bearup, L. A. (2019). Exploring source
544 water mixing and transient residence time distributions of outflow and evapotranspiration
545 with an integrated hydrologic model and Lagrangian particle tracking approach.
546 *Ecohydrology*, 12(1). <Go to ISI>://WOS:000454601400016
- 547 Maxwell, R. M., & Miller, N. L. (2005). Development of a coupled land surface and
548 groundwater model. *Journal of Hydrometeorology*, 6(3), 233-247. <Go to
549 ISI>://WOS:000230393600001
- 550 Miguez-Macho, G., & Fan, Y. (2025). A global humidity index with lateral hydrologic flows.
551 *Nature*, 644(8076), 413-419. <https://doi.org/10.1038/s41586-025-09359-3>
- 552 Mikkelsen, K. M., Maxwell, R. M., Ferguson, I., Stednick, J. D., McCray, J. E., & Sharp, J. O.
553 (2013). Mountain pine beetle infestation impacts: modeling water and energy budgets at
554 the hill-slope scale. *Ecohydrology*, 6(1), 64-72.
555 <https://doi.org/https://doi.org/10.1002/eco.278>
- 556 Piao, S. L., Wang, X. H., Park, T., Chen, C., Lian, X., He, Y., Bjerke, J. W., Chen, A. P., Ciais, P.,
557 Tommervik, H., Nemani, R. R., & Myneni, R. B. (2020). Characteristics, drivers and
558 feedbacks of global greening. *Nature Reviews Earth & Environment*, 1(1), 14-27.
559 <https://doi.org/10.1038/s43017-019-0001-x>
- 560 Pokhrel, Y., Felfelani, F., Satoh, Y., Boulange, J., Burek, P., Gädeke, A., Gerten, D., Gosling, S.
561 N., Grillakis, M., Gudmundsson, L., Hanasaki, N., Kim, H., Koutroulis, A., Liu, J.,
562 Papadimitriou, L., Schewe, J., Müller Schmied, H., Stacke, T., Telteu, C.-E.,... Wada, Y.
563 (2021). Global terrestrial water storage and drought severity under climate change.
564 *Nature Climate Change*, 11(3), 226-233. <https://doi.org/10.1038/s41558-020-00972-w>
- 565 Seager, R., Feldman, J., Lis, N., Ting, M., Williams, A. P., Nakamura, J., Liu, H., & Henderson,
566 N. (2018). Whither the 100th Meridian? The Once and Future Physical and Human
567



- 568 Geography of America's Arid–Humid Divide. Part II: The Meridian Moves East. *Earth*
569 *Interactions*, 22(5), 1-24. <https://doi.org/https://doi.org/10.1175/EI-D-17-0012.1>
- 570 Seager, R., Lis, N., Feldman, J., Ting, M., Williams, A. P., Nakamura, J., Liu, H., & Henderson,
571 N. (2018). Whither the 100th Meridian? The Once and Future Physical and Human
572 Geography of America's Arid–Humid Divide. Part I: The Story So Far. *Earth*
573 *Interactions*, 22(5), 1-22. <https://doi.org/https://doi.org/10.1175/EI-D-17-0011.1>
- 574 Shi, H., Jin, F.-F., Wills, R. C. J., Jacox, M. G., Amaya, D. J., Black, B. A., Rykaczewski, R. R.,
575 Bograd, S. J., García-Reyes, M., & Sydeman, W. J. (2022). Global decline in ocean
576 memory over the 21st century. *Science Advances*, 8(18), eabm3468.
577 <https://doi.org/doi:10.1126/sciadv.abm3468>
- 578 Swenson, L. J., Zipper, S., Peterson, D. M., Jones, C. N., Burgin, A. J., Seybold, E., Kirk, M. F.,
579 & Hatley, C. (2024). Changes in Water Age During Dry-Down of a Non-Perennial
580 Stream. *Water Resources Research*, 60(1), e2023WR034623.
581 <https://doi.org/https://doi.org/10.1029/2023WR034623>
- 582 Tan, X., Liu, B., & Tan, X. (2020). Global Changes in Baseflow Under the Impacts of Changing
583 Climate and Vegetation. *Water Resources Research*, 56(9), e2020WR027349.
584 <https://doi.org/https://doi.org/10.1029/2020WR027349>
- 585 Tran, H., Zhang, J., Cohard, J.-M., Condon, L. E., & Maxwell, R. M. (2020). Simulating
586 Groundwater-Streamflow Connections in the Upper Colorado River Basin. *Groundwater*,
587 58(3), 392-405. <https://doi.org/10.1111/gwat.13000>
- 588 Villaruel, A. J., Seck, A., & Schultz, C. (2025). Evaluating time-lagged relationships between
589 groundwater storage and river discharge using GRACE-based data: insights from the
590 Potomac Basin. *Environmental Research Communications*, 7(7), 075003.
591 <https://doi.org/10.1088/2515-7620/ade36f>
- 592 Visser, A., Thaw, M., Deinhart, A., Bibby, R., Safeeq, M., Conklin, M., Esser, B., & Van der
593 Velde, Y. (2019). Cosmogenic Isotopes Unravel the Hydrochronology and Water Storage
594 Dynamics of the Southern Sierra Critical Zone. *Water Resources Research*, 55(2), 1429-
595 1450. <https://doi.org/https://doi.org/10.1029/2018WR023665>
- 596 von Freyberg, J., Allen, S. T., Seeger, S., Weiler, M., & Kirchner, J. W. (2018). Sensitivity of
597 young water fractions to hydro-climatic forcing and landscape properties across 22 Swiss
598 catchments. *Hydrol. Earth Syst. Sci.*, 22(7), 3841-3861. [https://doi.org/10.5194/hess-22-
599 3841-2018](https://doi.org/10.5194/hess-22-3841-2018)
- 600 Wilusz, D. C., Harman, C. J., Ball, W. B., Maxwell, R. M., & Buda, A. R. (2019). Using particle
601 tracking to understand flow paths, age distributions, and the paradoxical origins of the
602 inverse storage effect in an experimental catchment. *Water Resources Research*, n/a(n/a),
603 e24397. <https://doi.org/10.1029/2019wr025140>
- 604 Xie, J., Liu, X., Jasechko, S., Berghuijs, W. R., Wang, K., Liu, C., Reichstein, M., Jung, M., &
605 Koirala, S. (2024). Majority of global river flow sustained by groundwater. *Nature*
606 *Geoscience*, 17(8), 770-777. <https://doi.org/10.1038/s41561-024-01483-5>
- 607 Yang, C., Maxwell, R., McDonnell, J., Yang, X., & Tijerina-Kreuzer, D. (2023). The Role of
608 Topography in Controlling Evapotranspiration Age. *Journal of Geophysical Research:*
609 *Atmospheres*, 128(18), e2023JD039228.
610 <https://doi.org/https://doi.org/10.1029/2023JD039228>
- 611 Yang, C., Maxwell, R. M., & Valent, R. (2022). Accelerating the Lagrangian simulation of water
612 ages on distributed, multi-GPU platforms: The importance of dynamic load balancing.



- 613 *Computers & Geosciences*, 166, 105189.
614 <https://doi.org/https://doi.org/10.1016/j.cageo.2022.105189>
615 Yang, C., Zhang, Y. K., Liang, X. Y., Olschanowsky, C., Yang, X. F., & Maxwell, R. (2021).
616 Accelerating the Lagrangian particle tracking of residence time distributions and source
617 water mixing towards large scales. *Computers & Geosciences*, 151. <Go to
618 ISI>://WOS:000641463100004
619 Yang, X., Tetzlaff, D., Soulsby, C., Smith, A., & Borchardt, D. (2021). Catchment Functioning
620 Under Prolonged Drought Stress: Tracer-Aided Ecohydrological Modeling in an
621 Intensively Managed Agricultural Catchment. *Water Resources Research*, 57(3),
622 e2020WR029094. <https://doi.org/https://doi.org/10.1029/2020WR029094>
623 Yang, Y., Roderick, M. L., Guo, H., Miralles, D. G., Zhang, L., Fatichi, S., Luo, X., Zhang, Y.,
624 McVicar, T. R., Tu, Z., Keenan, T. F., Fisher, J. B., Gan, R., Zhang, X., Piao, S., Zhang,
625 B., & Yang, D. (2023). Evapotranspiration on a greening Earth. *Nature Reviews Earth &*
626 *Environment*, 4(9), 626-641. <https://doi.org/10.1038/s43017-023-00464-3>
627 Zipper, S., Brookfield, A., Ajami, H., Ayers, J. R., Beightel, C., Fienen, M. N., Gleeson, T.,
628 Hammond, J., Hill, M., Kendall, A. D., Kerr, B., Lapides, D., Porter, M.,
629 Parimalarenganayaki, S., Rohde, M. M., & Wardropper, C. (2024). Streamflow Depletion
630 Caused by Groundwater Pumping: Fundamental Research Priorities for Management-
631 Relevant Science. *Water Resources Research*, 60(5), e2023WR035727.
632 <https://doi.org/https://doi.org/10.1029/2023WR035727>
633